NMR Characterization of Elastomer−Carbon Black Interactions

Gabriela Leu,[†] Yun Liu,[†] Denver D. Werstler,[‡] and David G. Cory*,[†]

Department of Nuclear Engineering, Massachusetts Institute of Technology, Cambridge, Massachusetts 02139, and Goodyear Research, Akron, Ohio 44305

Received March 31, 2004; Revised Manuscript Received June 29, 2004

ABSTRACT: Here we report the application of two-dimensional NMR double quantum filtered correlation spectroscopy to characterize the interactions between components in biphasic, heterogeneous media. The method was applied to model systems of carbon black reinforced rubber. The presence of filler particles induces local susceptibility fields while a local partial ordering of the elastomer at the surface prevents the complete averaging of the dipolar interaction. The separation of susceptibility and dipolar interactions allows for the direct observation of three elastomer components near the surface of filler particles: (1) encapsulated, (2) ordered surface layer, and (3) unordered layer near the surface. The NMR method permits one to quantify the amounts of elastomer in each of these regions and to estimate the thickness of the surface component. The method is applied to study several rubber samples for which the carbon black particle size distributions were determined from scanning electron microscopy measurements. For these samples the length scale of the surface elastomer component is estimated, and it is shown that the encapsulated elastomer is most probably located between the graphitic plates of the filler particles rather than in the space between adjacent particles.

I. Introduction

The unique physical and chemical properties of reinforced rubber make it one of the most important industrial materials. Reinforced rubber is a multicomponent, complex system made of carbon black particles (filler) and polymer chains. The long polymer molecules are responsible for its specific extensibility and elasticity, and the filler particles, in most cases carbon black (CB), improve the physical, mechanical, and electrical properties.[1−4] The complex carbon black−polymer and polymer−polymer interactions are responsible for the useful range of physical properties of rubber such as abrasion resistance, tensile stress at brake, and tear propagation resistance.

Despite numerous investigations of CB-filled elastomers by diverse techniques including dynamic, mechanical, thermal, and sorption analysis and spectroscopic methods, the molecular origin of the reinforcement effect is still under discussion.[1,2,5−9] NMR methods have also been used to study the matrix−filler interface (e.g., assessment of the degree of immobilization of rubber chains, extent of layer thickness, chain order, etc.)[10−22] and are commonly used to characterize mobility in heterogeneous polymer samples.[23−25] Previous studies on filled elastomers have shown that polymer chains have a strongly diminished mobility in the neighborhood of the filler particles.[12−17] Wang et al.[22] reported for the first time the use of ^{1}H multiple-quantum NMR for investigating the heterogeneity in segmental chain order of grafted polymers.

The main goal of our study is to develop two-dimensional NMR experiments for investigating the complex interactions in filled elastomers. We use the correlation of the local susceptibility fields that appear at the filler−polymer interface with the residual dipolar coupling due to partial ordering of the elastomer at the surface. This correlation probes both the surface structure and the mobility of the elastomer.

It has been suggested that there are three elastomer components in CB-filled rubber samples distinguished by their characteristic molecular mobility:[12,15,16,26,27] immobilized fraction, intermediate fraction, and mobile fraction. The immobilized fraction is the elastomer that is immobilized on the CB surface. It is trapped by the CB particles such that all the motions are restricted. The intermediate fraction is the elastomer located in the proximity of the surface of the CB particles, such that its dynamics is influenced by the presence of the CB particles. The mobile fraction is further from the CB particles such that the motions are not restricted and has the characteristics of bulk elastomers. The NMR method allows for the observation and measurement of the properties of three surface components in addition to the bulk free polymer.

A double quantum filter[21,28,29] is used to isolate the NMR signal from the elastomer with residual dipolar couplings. This corresponds to that elastomer that interacts with the CB particles, while the signal from the elastomer far from the CB, i.e., the bulk elastomer, is eliminated. In this way, the complex solid-state NMR spectra are simplified by observing only the relatively few elastomer protons that are in the immediate vicinity of the CB particles. The samples studied here are mainly bound rubber fractions from chemical extractions. Even in these concentrated samples the surface species we detect represent only about 1% of the total protons.

A. Properties of Rubber Samples. One primary CB particle is made of concentric layers whose graphitic order diminishes near the particle center.[30] The diameters of the CB particles vary from 10 to 100 nm. The surface of CB particles presents ordered zones of small graphitic crystallites joined by less ordered zones on which functional groups can be located. It can be considered that this is an intermediate state between amorphous carbon and the crystalline structure of graphite.

[†] Massachusetts Institute of Technology.
[‡] Goodyear Research.
* Corresponding author. E-mail: dcory@mit.edu.

10.1021/ma0493628 CCC: $27.50
Published on Web 08/11/2004

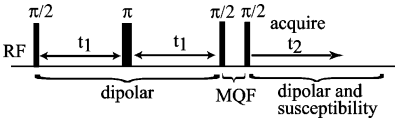

Figure 1. Double quantum filtering pulse sequence.

The polymer primarily used in this study was low vinyl polybutadiene (PBd). The characteristic dipolar interactions between ^{1}H atoms in a static, rigid molecule of PBd have strengths between 4 and 21 kHz. Fast, liquidlike intrachain motions average this interaction. However, in the filled polymer constraints imposed by the CB particles lead to a residual nonzero value for the dipolar coupling for the surface species where some degree of anisotropy is introduced. The magnitude of the ^{1}H−^{1}H dipolar coupling is observable in the NMR line shape which contains information about the local conformation of the elastomers. At the same time, the NMR signal is also influenced by the variation in the local magnetic field that arises due to differences in the local susceptibility induced by the presence of the CB particles. In this study the correlation of these two effects is measured. The dipolar interactions provide information on the local chain motions while the susceptibility shift provides a means to estimate the distance to the filler (CB) and the local geometry. The correlation between the dipolar and susceptibility interactions provides information on the chain orientation. The ^{1}H NMR signal from the rubber samples is due to the protons in the elastomeric chains. The vast majority of these protons are in elastomer chains that are not interacting intimately with the CB, and therefore, they are of no interest in this study. However, they mask the desired information regarding the CB−elastomer interactions. This is true even in bound rubber fractions where a great deal of molecular mobility still exists. A double quantum filter removes these undesired signals.

B. DQF Dipolar/Susceptibility Spectroscopy. We use a two-dimensional correlation spectroscopy pulse sequence with double quantum filtering.[31] The pulse sequence is shown in Figure 1. This sequence refocuses the susceptibility interaction in the first dimension, so during the evolution time t_1 the spins can be considered as evolving only due to dipolar interactions. The 180° pulse refocuses the effect of the time-independent susceptibility fields. The multiple quantum filter ensures that the final signal is only due to spins that are dipolarly coupled during t_1, strongly diminishing the signal from the bulk elastomer which would otherwise mask the signals of interest in our system. In the second dimension (i.e., during the acquisition time t_2), the spins evolve under both dipolar and susceptibility fields. In this way, we observe the correlation between the dipolar and susceptibility fields while the signal from the free elastomer is strongly attenuated. Double Fourier transformation of $S(t_1,t_2)$ leads to the two-dimensional NMR-DQF spectrum $S(\omega_1,\omega_2)$. The two-dimensional spectra obtained with this pulse sequence represent the strength of the remaining dipolar interaction along one axis and a combination of the dipolar and susceptibility interactions along the other axis. The symmetry about $f_1 = 0$ is a consequence of the type of Fourier transform and contains no additional information.

A typical spectrum is shown in Figure 2 in which we identify three components. We distinguish the components based on the relative strengths of the susceptibility and dipolar interactions. We will identify these by their compositional assignments which we will justify in the remainder of the paper. Every filled sample we have studied has a component with a well-resolved dipolar interaction and no appreciable susceptibility shift. This is the diagonal component in the figure. Since the elastomer used in our samples was not cross-linked, this component is practically absent when filler particles are not present. Therefore, we assign this to encapsulated polymer (also known as "occluded rubber") where the susceptibility interaction is suppressed by symmetry. This polymer is roughly symmetrically surrounded by CB. The dipolar interaction does not vanish for the encapsulated material since the small space it occupies restricts its reorientation. The second component sees both dipolar and susceptibility interactions of roughly the same strength. This we assign to an ordered surface layer where the susceptibility arises from the CB−polymer interface and the dipolar interaction remains due to surface ordering. The third component we characterize as an unordered near surface layer; it has a large susceptibility shift and a small dipolar interaction. We expect that the susceptibility effect falls off more slowly than the polymer ordering as one moves away from the interface. So this material is only very weakly (if at all) ordered and has extensive local motion, but not enough motional freedom to sample a wide range of susceptibility fields. Recall that the CB particles have diameters of tens of nanometers.

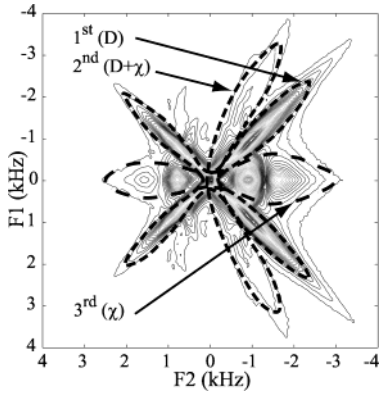

Figure 2. Typical 2D NMR-DQF spectral correlation map (sample X-110) of dipolar (F_1) vs dipolar and susceptibility (F_2) interactions. The three distinct spectral components used in our analysis are emphasized (dotted lines).

Although reinforced rubber is an extremely complex and heterogeneous material, we can still learn about the average local structure and length scales from very simple spectral simulations. For example, the line shape of the surface component is a function of (1) the relative orientations of the dipolar and susceptibility principal axis systems (PAS) and (2) the relative strengths of the dipolar and susceptibility fields.

We make the simplifying assumption that the dipolar interaction can be reduced to one axially symmetric powder pattern, thereby reducing the couplings of many spins to effectively just a spin pair. For the susceptibility interaction we make the reasonable approximation that this too is axially symmetric and then simulate the expected 2-D spectrum for a variety of angles between the PAS.[32] The results of these simulations are shown in Figure 3. By comparing these theoretical simulations with experimental results, we infer that these two PAS are almost parallel for all of our samples (e.g., see Results, Figure 6).

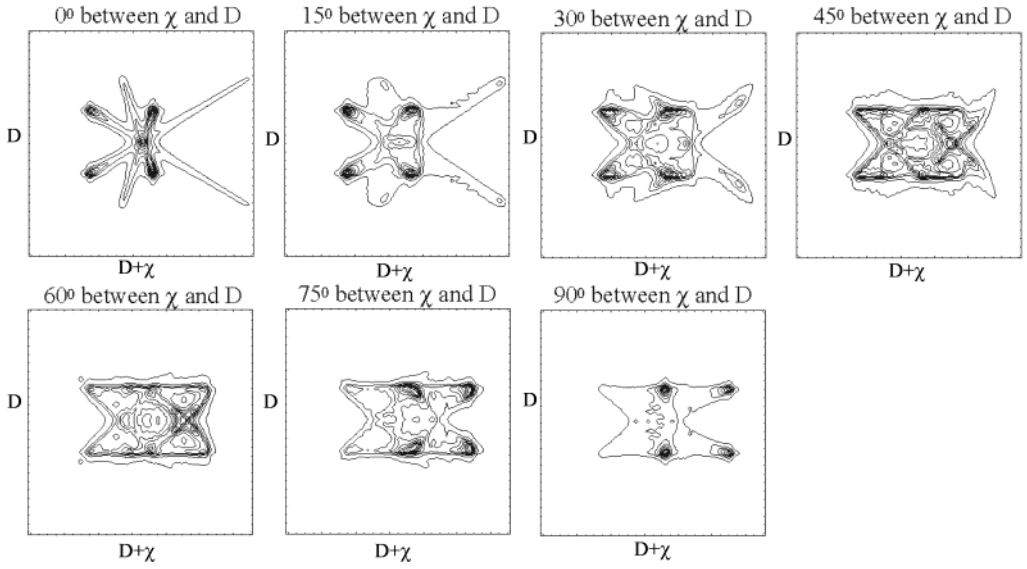

Figure 3. Simulation results showing the 2D spectra obtained for different orientations of the PAS between the dipolar and susceptibility tensors. The simulation with 0° between the PAS of the dipolar and susceptibility tensors is in very good agreement with the experimental data.

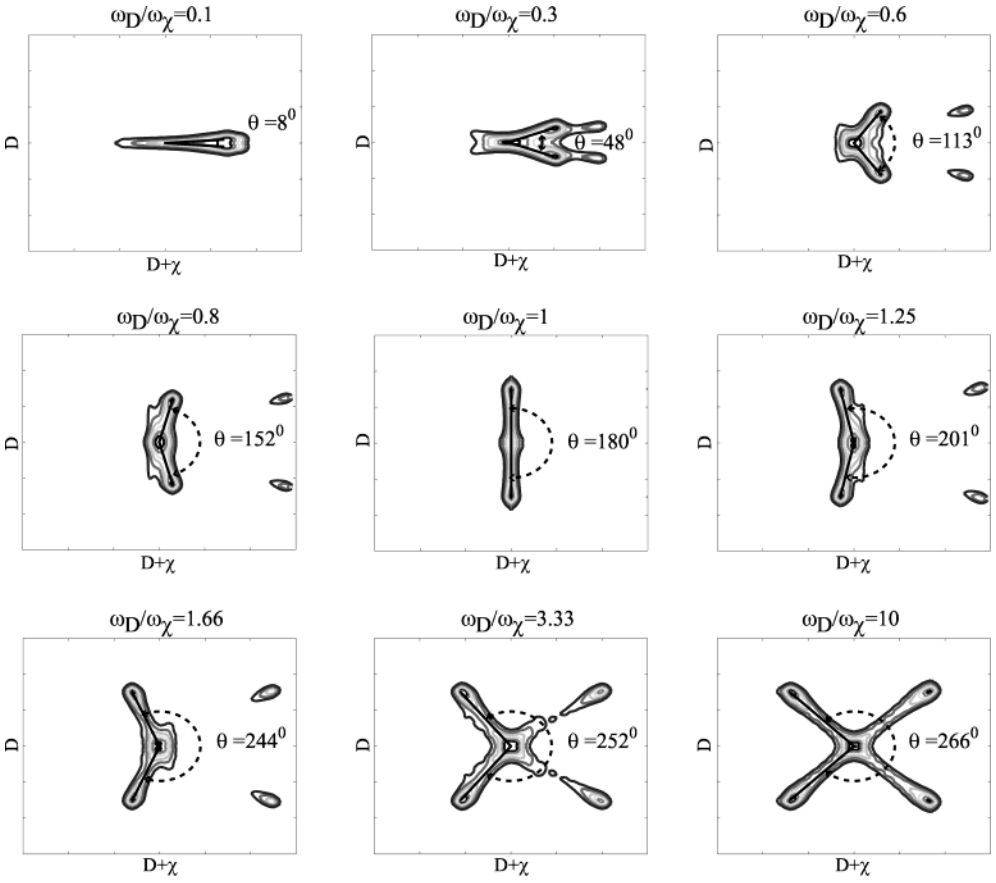

Figure 4. Simulations results showing the variation of the angle θ between the most intense peaks corresponding to the second component for different relative strengths of the dipolar and susceptibility fields. The contour levels were chosen to emphasize only the strongest component for which we measure the θ angle.

The relative contribution of the local dipolar ω_D and susceptibility ω_χ fields is obtained by monitoring the angle θ between the most intense peaks for several relative strengths of the dipolar and susceptibility fields. Simulation results are shown in Figure 4 for $0.1 < \omega_D/\omega_\chi < 10$. The sensitivity of this analysis is shown in Figure 5. For all of the samples where an ordered surface species is observed, the angle θ is about 132°, corresponding to $\omega_D/\omega_\chi = 0.7$ at 12 T. Of course, the susceptibility shift is field dependent, and we have also run experiments at 7 T to verify this. A single type of carbon black was used in all sample preparations, and so this consistency is expected.

We quantify the relative amounts of the three components by simulating the overall powder pattern. Since there are spectral regions that are unique for each component, this is fairly accurate. In addition, we extract the second moments of the line shapes.

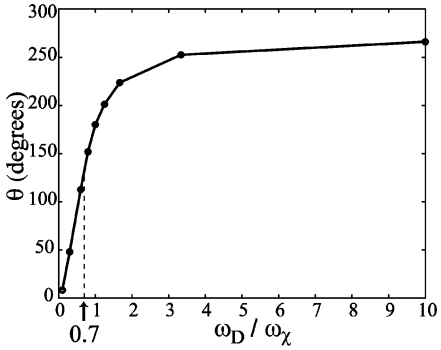

Figure 5. Variation of θ with ω_D/ω_χ.

II. Experimental Section

The rubber samples used in this study are described in Table 1.

The PBd's in this study were prepared with *n*-BuLi initiator without modifier, resulting in a microstructure of 51% *trans*-1,4, 39% *cis*-1,4, and 10% 1,2. The molecular weight for these samples was approximately 200K. The functionalized PBd was end-capped with tributyltin by adding tributyltin chloride. 40 phr of CB779 was added to each sample.

The SBR's in the SBR−PI blends in this study were experimental and were prepared with *n*-BuLi initiator and *N*′,*N*′,*N*,*N*-tetramethylethylenediamide (TMEDA) polar modifier. Final composition/microstructure was approximately 23% styrene, 24% *trans*-1,4-BD, 17% *cis*-1,4-BD, 33% 1,2-BD, and 3% substituted divinylcyclohexane by weight. The latter structure is discussed in ref 33. The functionalized SBR was end-capped with tributyltin by adding tributyltin chloride. The PI's in the SBR−PI samples were Natsyn 2200, a commercially available Ziegler−Natta-catalyzed synthetic high-cis (97%) polyisoprene made by Goodyear Tire & Rubber Co. 40 parts of CB779 was added to 80 parts of the SBR and 20 parts of the PI. The samples were mixed in a Haake Rheocord mixer held at 100 °C and were mixed for 3 min at 55 rpm. A typical

Table 1. Sample Properties

sample	polymer	filler level (phr)	brf[a]	functionalized[b]
X-110	PBd[c]	70	X	−
X-120	PBd	79	X	X
X-130	PBd	213	X	−
X-200	PBd	160	X	−
X-220	PBd	160	X	−
X-285	PBd	40	−	−
Z-350	80/20 SBR/PI[d]	96	X	−
Z-355	80/20 SBR/PI	173	X	SBR
Z-390	80/20 SBR/PI	40	−	SBR

[a] Bound rubber fraction. [b] Terminally functionalized SBR or PBd. [c] PBd is a low vinyl polybutadiene. The microstructure is 51 trans, 39 cis, 10 vinyl. [d] PI is a Natsyn 2200, a 98% cis synthetic polyisoprene. The SBR is a 23 wt % styrene solution SBR. See the Experimental Section for details.

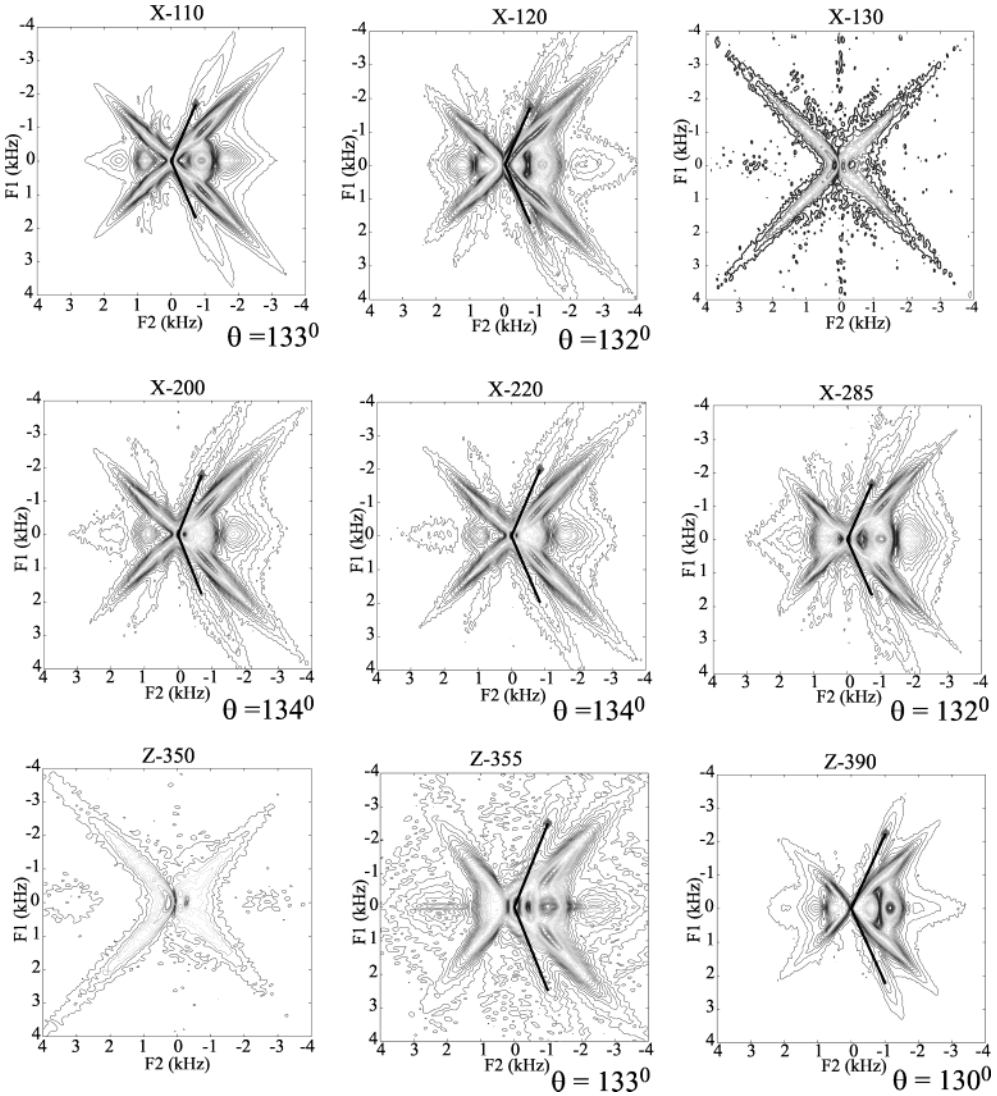

Figure 6. Results of 2D NMR-DQF experiments for all the samples used in this study. The angle θ between the most intense peaks corresponding to the second component is shown, and it is observed to be close to 132° for all the samples.

Table 2. Experimental Results: Second Moments ($\sqrt{M_2}$) and the Percent Fraction of Unordered (P_{unord}), Surface (P_{surf}), and Encapsulated (P_{enc}) Elastomer Components[a]

sample	$\sqrt{M_2}$ (Hz) F_1 proj	$\sqrt{M_2}$ (Hz) extr unord	$\sqrt{M_2}$ (Hz) extr dip	$P_{enc+surf}$	I_{enc}/I_{surf}	θ	P_{unord}	P_{surf}	P_{enc}
X-110	1718	478	1529	83	4.54	133	17	15	68
X-120	1537	592	1619	82	2.54	132	18	23	59
X-130	1670			100			0	0	100
X-200	1568	592	1608	89	2.78	134	11	24	65
X-220	1615	592	1661	87	3.37	134	13	20	67
X-285	1540	478	1332	88	2.84	132	12	23	65
Z-350	1390	550	1787	98					
Z-355	1190	552	1515	87	2.16	133	13	28	59
Z-390	1440	592	1493	58	2.34	130	42	17	41

[a] The second moments correspond to the line shapes of the projections of the 2D spectra on the F_1 axis (F_1 proj), to the extracted line shape of the unordered component from the F_1 projection (extr unord), and to the remaining F_1 projection after subtracting the unordered component (extr dip). θ is the angle between the most intense peaks of the surface component. I_{enc}/I_{surf} is the ratio of the maximum intensities peaks in the encapsulated and surface components, used in estimating the percent fraction of elastomer components.

batch size was 50 g. The mixed batch was then milled (three passes).

For the bound rubber preparation each sample was cut into pieces approximately 1 mm wide (both dimensions) and 4−5 mm long. These pieces were placed in a stainless steel basket (with a loop handle) with dimensions of about 1.5 mm (deep) × 1.5 mm (wide) × 6.5 mm (long). About 1 g of sample was placed in each of the two baskets that were then placed in a resin kettle with 400 mL of toluene. The solution was placed under a blanket of nitrogen and was very slowly agitated by a magnetic stirring bar. The samples were extracted for 3 days, at which point the solvent and soluble polymer were removed, and a fresh 400 mL of toluene was placed in the kettle to further extract the rubber samples. After the second 24 h extraction, the solvent and soluble rubber were again removed. The insoluble bound rubber fraction was washed into an aluminum pan with hexane. 2−3 drops of Paratax antioxidant were added before the solvent was evaporated. The bound rubber fraction was vacuum-dried and then weighted. Typically, 95 wt % of soluble polymer was removed during the first extraction.

For sample selection, emphasis was placed on establishing a foundation for the understanding of the elastomer−filler interaction as opposed to a comprehensive study for different types of elastomers. Both low vinyl polybutadienes (samples X-110, X-120, X-130, X-200, X-220, and X-285) and SBR−PI blends (sample code Z-350, Z-355, and Z-390) were studied. Three of these, X-120 (PBd), Z-355 (SBRPI), and Z-390 (SBRPI), were functionalized. Unless otherwise stated, the experiments were run on bound rubber fractions (after the toluene-soluble portion of the elastomer was extracted; this process effectively increases the CB concentration by a significant amount which depends on how much rubber was extracted) in order to eliminate as much as possible the noninteracting elastomer. Carbon black 779 (CB 779) was used exclusively to eliminate the CB type as a factor. This CB is a N229 ISAF reinforcing black with high surface structure (124 $cm^3/100$ g) and surface area (108 m^2/g). The surface structure characterizes the empty space between randomly packed aggregates of carbon black. The data for the CB surface structure were obtained by the standard DBP (dibutyl phthalate) method.

The experiments were performed on a Bruker DRX500 spectrometer at a ^1H frequency of 500.13 MHz. The pulse sequence in Figure 1 was used. The 90° pulse length was 4.5 μs, and recycle delays of 3 s were used. The t_1 time was varied from 3 μs to 3.2 ms in increments of 25 μs, and the delay between the second and third 90° pulses was 3 μs. The dead time of the spectrometer was 7.14 μs. All measurements were carried out at room temperature (20 °C).

The 2-D spectra for all samples are shown in Figure 6.

The experimental results are summarized in Table 2.

To quantify the relative amounts of elastomers that are responsible for the encapsulated and surface components, we simulated numerically the 2D NMR-DQF spectra. The simulations were performed for the case when the amounts of molecules that feel only dipolar interactions (i.e., encapsulated component) is equal to the amount of molecules responsible for the surface component. The ratio of the maximum intensity peaks that define these components is measured to be 1.45. We extracted the corresponding peaks intensity ratio from the experimental data. Besides this ratio, we estimated from the projections of the 2D data the fraction from the total signal that corresponds to the encapsulated and surface components. From this system of two equations with two unknowns we estimated the amounts of encapsulated and surface elastomer components. The unordered component corresponds to the remaining fraction up to 100%. These relative values could be useful for the comparative characterization of the samples. Table 2 shows the relative amounts of encapsulated, surface, and unordered elastomer components. The surface and unordered components are either present together or not present at all (e.g., sample X-130). The unextracted Z-390 sample has the largest relative amount of unordered component and the smallest amount of encapsulated component. These results show that it is possible to use our method for extracting information on the relative amounts of the three elastomer components in rubber samples. A more systematic study is necessary for quantifying the relation between the relative amounts of elastomer components and the physical properties of the rubber samples.

A. NMR Susceptibility Measurements of Carbon Black. To characterize the CB, we measure the susceptibility difference between it and dimethyl sulfoxide (DMSO) in a MAS NMR experiment.[34] The spectrum of DMSO mixed with CB powder shows both a narrow line from DMSO in the center of the rotor that does not see the CB and a broad line due to the DMSO trapped between the CB particles. The peak is broadened due to the susceptibility field which remains under MAS since the DMSO is surrounded on all sides by the CB. The splitting between these two peaks is 196 Hz for the CB779 in a 500 MHz spectrometer. The observed signal splitting is

$$\Delta\nu = \frac{2}{3}\nu_0\Delta\chi \qquad (1)$$

where $\nu_0 = \gamma B_0$ is the main static magnetic field and $\Delta\chi$ is the susceptibility difference between CB and DMSO. From the measured splitting we calculate the susceptibility difference between CB and DMSO to be $\Delta\chi = 6.15 \times 10^{-6}$.

B. Estimation of CB Particle Sizes: SEM Experiments. To characterize the spatial width of the surface layer and the location of the encapsulated material, it is helpful to have an accurate estimation of the CB particle size. We explored atomic force microscopy (AFM),[30,35] scanning electron microscopy (SEM),[30,36−38] and transmission electron microscopy (TEM)[30,39] imaging experiments to investigate the CB particles in our samples. SEM provided the best results for our samples because of their relatively soft consistency which made the preparation of optimal probes for AFM and TEM difficult. In the case of SEM the sample preparation is not as critical, and

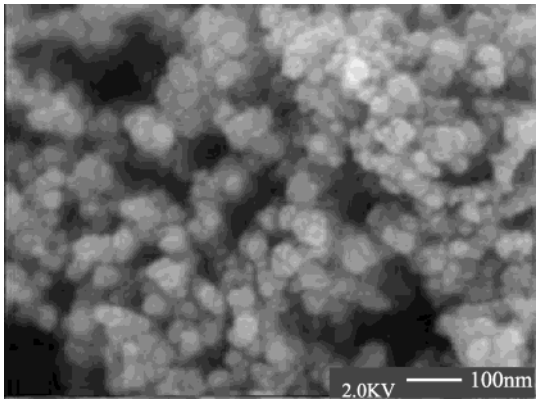

Figure 7. SEM image of the carbon black powder. The mean diameter of the CB particles is 35 ± 4.5 nm.

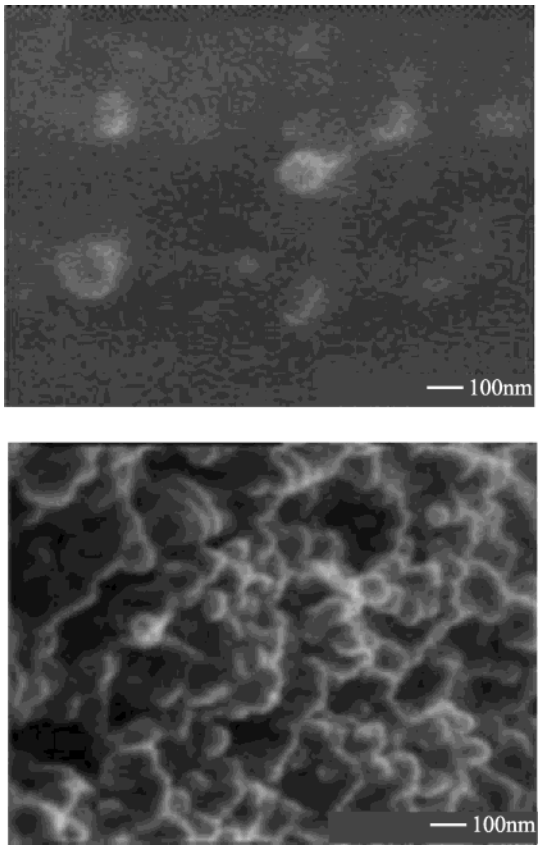

Figure 8. SEM images of the X-110 PBd sample (top) and of the X-130 PBd sample (bottom). For X-110, the mean diameter of the CB particles is 110 ± 17 nm. For the X-130 sample, the mean diameter of the CB particles is 83 ± 9.7 nm.

a clear distinction of the CB particles is obtained as they have a significantly higher atom density compared to the elastomer.

Figure 7 shows a typical SEM image obtained for the CB powder, without elastomer. From this image we estimate the average size of the CB particles before mixing with the elastomer to be 35 ± 4.5 nm.

Figure 8 (top) presents SEM results for the X-110 PBd sample which has a relatively small concentration of CB. The average diameter in this case is 110 ± 17 nm.

The SEM image for the X-130 PBd sample which has the highest concentration of CB particles is shown in Figure 8 (bottom). The average diameter in this case is 83 ± 9.7 nm.

The CB mean diameters as seen in the SEM measurements are summarized in Table 3 along with the concentrations of the three NMR distinct elastomer components.

The pure CB particles have a significantly smaller mean diameter than the CB particles in the bound rubber fractions. Recall that the elastomer is not seen in these images.

Table 3. Estimations of Mean Diameters of CB Particles Derived from SEM Experiments

sample	P_{unord}	P_{surf}	P_{enc}	N^a	CB mean diameter (nm)
CB779	NA[b]	NA	NA	153	34.9 ± 4.5
X-110	17	15	68	6	111.3 ± 17.4
X-285	12	23	65	30	68.8 ± 8.6
Z-355	33	28	59	13	48.0 ± 9.7
X-130	0	0	100	17	82.9 ± 9.7

[a] Number of CB particles considered. [b] No polymer present.

These measurements suggest that some elastomer effectively swells the CB particles. In addition, the NMR results show that the functionality of the elastomer may have an effect on the final CB particle size. For example, for sample Z-355, whose main difference from the others is that the elastomer is functionalized and contains styrene, we measure smaller diameters than for the other rubber samples, yet still larger than for pure CB. Nonfunctionalized styrene-containing elastomers would have to be studied to verify this, as the styrene–CB interaction would be expected to be strong.

III. Discussion

We have already seen that the NMR method can suppress the free elastomer signal and permits the observation of three unique elastomer/CB components based on local correlations of the dipolar and susceptibility interactions. The model we suggest for the three components is an encapsulated species that is held in small regions within the CB particle and is effectively completely surrounded by CB, an ordered surface species, and an unordered species far enough from the surface so that it has additional mobility and is not ordered, yet near enough to feel the full susceptibility field of the CB particle. The NMR results provide a quantitative measure of these three components in the bound rubber fractions studied.

Some of the additional questions we wish to explore are (1) to estimate how thick the surface layer is, (2) to determine the location of the encapsulated material, and (3) to measure the spatial extent of the unordered material.

A. Thickness of the Ordered Surface Layer. Given the diameter of the CB particle as measured by SEM, we can estimate the width of the surface layer by comparing the susceptibility line shape to that calculated for a spherical shell. Since we have measured the bulk magnetic susceptibility of the CB, this is a well-characterized problem. The field near the surface of the CB particle is not uniform. For a homogeneous sphere of susceptibility χ, the susceptibility field outside the sphere, in polar coordinates, is given by[40]

$$\mathbf{B}(\mathbf{r},\theta) = B_0\left[\left(1 + \frac{2a^3}{r^3}\frac{\mu_{int} - \mu_{ext}}{\mu_{int} + 2\mu_{ext}}\right)\cos\theta\cdot\mathbf{i}_r - \left(1 - \frac{a^3}{r^3}\frac{\mu_{int} - \mu_{ext}}{\mu_{int} + 2\mu_{ext}}\right)\sin\theta\cdot\mathbf{i}_\theta\right] \quad (2)$$

where a is the radius of the CB particle. The value that we use in our calculations is the value that we determined from the SEM measurements. μ_{int} and μ_{ext} are the permeabilities of the CB particle and of the surrounding medium, respectively; B_0 is the external applied static magnetic field. The relation between the permeability and the magnetic susceptibility is

$$\mu = \mu_0(1 + \chi) \quad (3)$$

Knowing the susceptibility difference between the CB

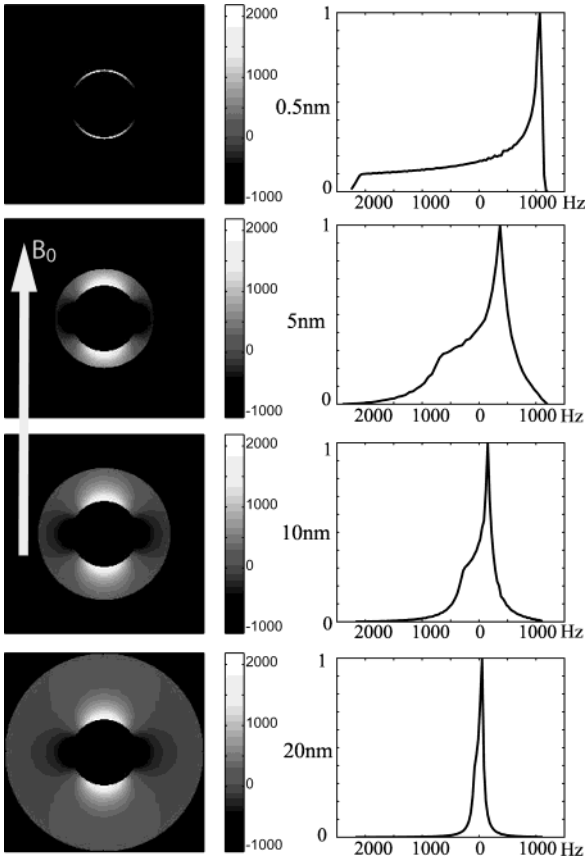

Figure 9. Simulation results showing the field distribution in spherical shells of different thickness around the CB particle.

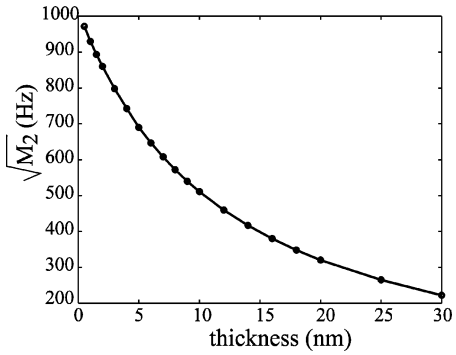

Figure 10. Dependency of the second moment of the field distribution as a function of the shell thickness.

particles and their surrounding medium (elastomer), we can estimate the local field around the CB particles. On the basis of these estimations, we can calculate the magnetic field distribution in spherical shells of various widths around the CB particle (Figure 9). Since the field falls off as $1/r^3$, the thicker the surface layer the narrower the distribution. From these simulations, we correlate the second moments (M_2) of these field distributions to the various corresponding widths of each shell, and we obtain the "calibration" curve shown in Figure 10. From the experimental $\sqrt{M_2}$ values we estimate the approximative thickness of the ordered surface elastomer layer to be between 1 and 3 nm. It should be noted that the surface layer is either present at roughly the same level or it is entirely absent (e.g., sample X-130). Likewise, the square root of the second moment of the susceptibility interaction is roughly

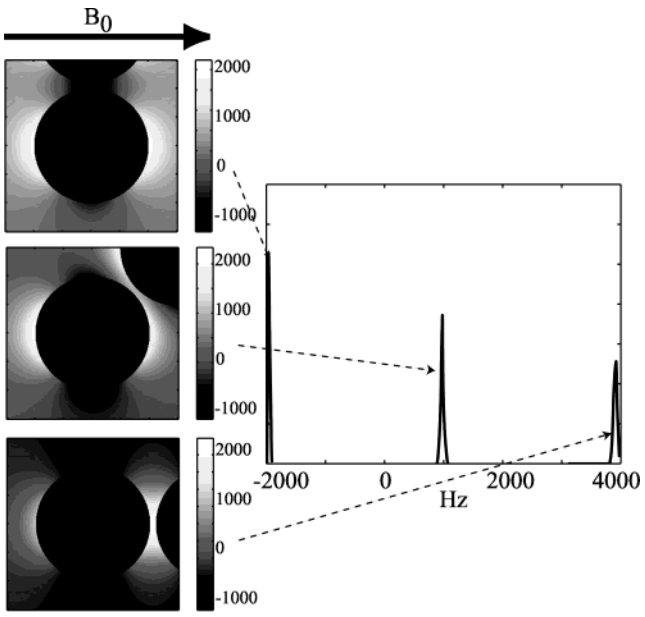

Figure 11. Simulation results for two spheres showing the field distribution in a small volume between the CB particles. The diameter of the CB particles is 35 nm, and the distance between their centers is 37 nm. The magnetic field distribution is calculated in a cubic volume element centered at the half distance between the two spheres and with edge length of 3 nm.

constant for those samples that have a surface component.

B. Location of the Encapsulated Elastomer. We would like to justify our suggestion that the encapsulated elastomer is swelling the CB particles, and it is not in the interstitial space between the spherical CB particles. Here we remind the reader that, even if the CB particles are tightly packed, the material in the spaces between particles still sees an appreciable variation in the susceptibility field. When this fact is combined with our observation from SEM that in the presence of elastomer the CB particles swell, we are left to conclude that the encapsulated material must be within the CB particles.

As we have seen from the SEM experiments (e.g., Figure 8, bottom), it is very common to have adjacent CB particles rather than single, isolated particles. So we estimate the field distribution in a small region between the CB particles. We start by using two particles. As shown in Figure 11, for two spheres, large field susceptibility variations occur at these locations for various orientations with respect to the external magnetic field B_0. Because the volume investigated is relatively small, the field distributions are quite narrow. However, there is a broad range of field values if we consider the entire sample with all the possible orientations, and therefore, the space between two spheres is not a probable location for the encapsulated elastomer.

A more realistic case is to consider the space inside clusters of three and even five spheres, tangent to each other. For three spheres the simulated field distribution is still quite broad (Figure 12). Even for five spheres we observe that the simulated distributions are still very broad, only slightly narrower than for the case of three spheres.

All these simulation results suggest that the encapsulated component, since it does not feel susceptibility variations, is probably not trapped between the CB

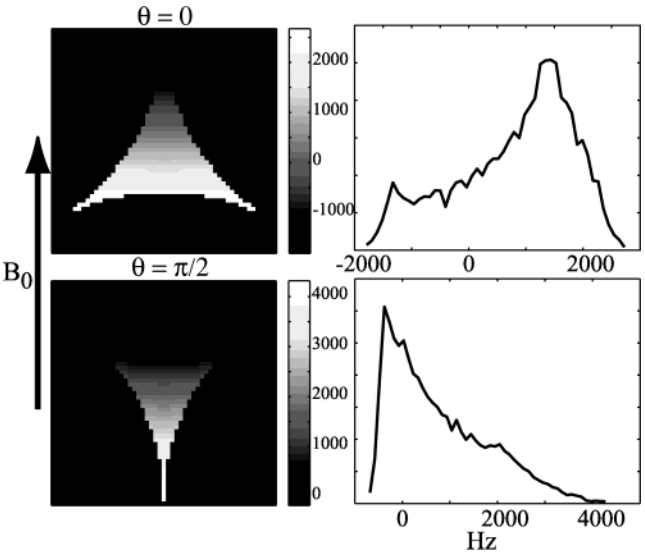

Figure 12. Simulation results for three spheres showing the field distribution in the space between the CB particles. The diameter of the CB particles is 35 nm, and they are tangent to each other.

particles. This observation coupled with the information from the SEM measurements suggests that the encapsulated elastomer is rather trapped between the shells of the CB particles themselves, inducing the increase of their effective radius as observed by SEM. The currently accepted model for CB particles which was proposed by Heidenreich et al.[41] from TEM studies allows for the possibility of a specific CB/elastomer interaction in which the elastomers disrupt the ordered semicrystalline structure of the graphitic ordered plates at the surface of CB particles, producing an increase of their effective volume. The average spacing measured by electron microscopy, between the CB graphitic layers, is about 0.4 nm.[41]

C. Thickness of the Unordered Surface Layer. There is little additional information to give about the unordered surface layer. We assume that it is contiguous with the ordered surface layer. If we follow the same procedure to calculate the susceptibility shifts as for the ordered surface layer, we can build a "calibration" curve for the second moments of the field distributions for the unordered component. We assume for these calculations an average thickness of the ordered surface layer of 2 nm, and the thicknesses of the unordered component is constrained by the susceptibility to be between 0.5 and 8.0 nm. Using the experimental estimation of the line shape of the axially asymmetric powder pattern, we find a most probable width range of the unordered phase between 0.5 and 2.0 nm. In all but one case (sample Z-390) there is less unordered surface material than ordered, and so an estimation of 1−2 nm thickness seems reasonable. Since the local change in the susceptibility field with distance from the surface is small once you are some distance from the surface, the susceptibility shift is not a very accurate means of determining the width of the unordered layer.

IV. Conclusions

We have applied two-dimensional NMR-DQF correlation spectra to the study of reinforced rubber. Three elastomer components are identified: an encapsulated material, an ordered surface layer, and an unordered near surface layer. We suggest that the encapsulated material effectively swells the CB particles and is located in the interior of these. The surface layer appears to have an average chain configuration (corresponding to the PAS of the dipolar tensor) ordered perpendicularly to the surface and is approximately 2 nm thick. The unordered near surface layer is assumed to be contiguous with the ordered surface layer and is somewhat thinner in bound rubber but is significantly thicker for whole reinforced rubber samples.

We have quantified the amounts of each component in a variety of samples. We observe that all samples regardless of treatment include an encapsulated component. For some preparations chemical extraction of the soluble rubber is able to remove both surface layers (sample X-130). We have never observed an ordered surface layer without also observing an unordered layer.

Although our initial studies focused on bound rubber fractions to reduce the interference from free elastomer, we observe that the multiple-quantum filter is selective enough to permit whole reinforced rubber samples to be studied.

It is apparent that both the surface layers and the interpenetration of the elastomer into the CB contribute to the structural and mechanical properties of reinforced elastomers. We anticipate that these NMR methods will help to sort out the particular properties of each.

Acknowledgment. We acknowledge support from Goodyear Tire and Rubber Co. and from the National Science Foundation.

References and Notes

(1) Kraus, G., Ed.; *Reinforcement of Elastomers*; Wiley and Sons: New York, 1965.
(2) Donnet, J. B.; Voet, A. *Carbon Black Physics, Chemistry and Elastomer Reinforcement*; M. Dekker, New York, 1976.
(3) Donnet, J. B.; Vidal, A. *Adv. Polym. Sci.* **1986**, *76*, 103.
(4) Vidal, A.; Donnet, J. B. *Colloid Polym. Sci.* **1987**, *75*, 201.
(5) Plinskin, L.; Tokita, N. *J. Appl. Polym. Sci.* **1972**, *16*, 473.
(6) Wang, M. J.; Wolff, S. *Rubber Chem. Technol.* **1992**, *65*, 890.
(7) Donnet, J. B. *Compos. Sci. Technol.* **2003**, *63*, 1085.
(8) Nikiel, L.; Gerspacher, M.; Yang, H.; O'Farrell, C. P. *Rubber Chem. Technol.* **2001**, *74*, 249.
(9) Wolff, S.; Wang, M. J.; Tan, E. H. *Rubber Chem. Technol.* **1993**, *66*, 163.
(10) Honnold, V. R.; McCaffery, F.; Mrowca, B. A. *J. Appl. Phys.* **1954**, *25*, 1219.
(11) Schaefer, J. *Macromolecules* **1973**, *6*, 882.
(12) O'Brien, J.; Cashell, E.; Wardell, G. E.; McBrierty, V. J. *Macromolecules* **1976**, *9*, 653.
(13) Wardell, G. E.; McBrierty, V. J.; Marsland, V. *Rubber Chem. Technol.* **1982**, *55*, 1095.
(14) Huijgen, T. P.; Angad Gaur, H.; Weeding, T. L.; Jenneskens, L. W.; Schuurs, H. E. C.; Huysmans, W. G. B.; Veeman, W. S. *Macromolecules* **1990**, *23*, 3063.
(15) Kenny, J. C.; McBrierty, V. J.; Rigbi, Z.; Douglass, D. C. *Macromolecules* **1991**, *24*, 436.
(16) Litvinov, V. M.; Steeman, P. A. M. *Macromolecules* **1999**, *32*, 8476.
(17) Mansencal, R.; Haidar, B.; Vidal, A.; Delmotte, L.; Chezeau, J. M. *Polym. Int.* **2001**, *50*, 387.
(18) Blümler, P.; Blümich, B. *Acta Polym.* **1993**, *44*, 125.
(19) Sperling, K.; Veeman, W. S. *J. Braz. Chem. Soc.* **1999**, *10*, 299.
(20) Pellicioli, L.; Mowdood, S. K.; Negroni, F.; Parker, D. D.; Koenig, J. L. *Rubber Chem. Technol.* **2002**, *75*, 65.
(21) Graf, R.; Heuer, A.; Spiess, H. W. *Phys. Rev. Lett.* **1998**, *80*, 5738.
(22) Wang, M.; Bertmer, M.; Demco, D. E.; Blümich, B.; Litvinov, V. M.; Bathel, H. *Macromolecules* **2003**, *36*, 4411.
(23) Buda, A.; Demco, D. E.; Bertmer, M.; Blumich, B.; Litvinov, V. M.; Penning, J. P. *J. Phys. Chem. B* **2003**, *107*, 5357.
(24) Dollase, T.; Graf, R.; Heuer, A.; Spiess, H. W. *Macromolecules* **2001**, *34*, 298.
(25) Landfester, K.; Spiess, H. W. *Acta Polym.* **1998**, *49*, 451.

(26) Lüchow, H.; Breier, E.; Gronski, W. *Rubber Chem. Technol.* **1997**, *70*, 747.
(27) McBrierty, V. J.; Packer, K. J. *Nuclear Magnetic Resonance in Solid Polymers*; Cambridge University Press: New York, 1993.
(28) Bodenhausen, G.; Vold, R. L.; Vold, R. R. *J. Magn. Reson.* **1980**, *37*, 93.
(29) Jaccard, G.; Wimperis, S.; Bodenhausen, G. *J. Chem. Phys.* **1986**, *85*, 6282.
(30) Donnet, J. B.; Bansal, R. C.; Wang, M.-J. *Carbon Black: Science and Technology*; M. Dekker: New York, 1993.
(31) Ernst, R. R.; Bodenhausen, G.; Wokaun, A. *Principles of Nuclear Magnetic Resonance in One and Two Dimensions*; Oxford University Press: Oxford, 1994.
(32) Schmidt-Rohr, K.; Spiess, H. W. *Multidimensional Solid-State NMR and Polymers*; Academic Press: London, 1994.
(33) Henning, S. K.; Werstler, D. D.; Kerns, M. L.; Ofstead, E. A. Rubber Division, American Chemical Society Meeting, Pittsburgh, PA, Oct 2002.
(34) Chen, J.-H.; Enloe, B. M.; Cory, D. G.; Singer, S. *Magn. Reson. Med.* **2003**, *50*, 515.
(35) Binning, G.; Quate, C. F.; Gerber, C. *Phys. Rev. Lett.* **1986**, *56*, 930.
(36) Crewe, A. V.; Wall, J. *Proceedings of the Electron Microscopy Society of America*, 27th Annual Meeting, St. Paul, MN, 1969; p 172.
(37) Nomura, S.; Todekoro, H.; Komoda, T. *Proceedings of the Electron Microscopy Society of America*, 34th Annual Meeting, Miami Beach, FL, 1976; p 524.
(38) Ray, I. L. F.; Drummond, I. W.; Banbury, J. R. *Developments in Electron Microscopy and Analysis*; Academic Press: London, 1976; p 11.
(39) Hess, W. M.; Ban, L. L.; McDonald, G. C. *Rubber Chem. Technol.* **1969**, *42*, 1209.
(40) Jackson, J. D. *Classical Electrodynamics*; John Wiley and Sons: New York, 1999.
(41) Heidenreich, R. D.; Hess, W. M.; Ban, L. L. *J. Appl. Crystallogr.* **1968**, *1*, 1.

MA0493628